


Dynamical magnetoelectric coupling in axion insulator thin films

Zhaochen Liu,¹ Jiang Xiao^{1,2} and Jing Wang^{1,2,3,*}

¹State Key Laboratory of Surface Physics and Department of Physics, Fudan University, Shanghai 200433, China

²Institute for Nanoelectronic Devices and Quantum Computing, Fudan University, Shanghai 200433, China

³Zhangjiang Fudan International Innovation Center, Fudan University, Shanghai 201210, China

 (Received 3 September 2020; revised 16 December 2021; accepted 10 June 2022; published 21 June 2022)

The *quantized* topological magnetoelectric effect (TME) is the hallmark of the axion insulator but remains unexplored due to its small signal. In axion insulator thin films, TME deviates from the exact quantization due to the finite-size effect. Here we show that such finite-size correction depends on the *out-of-plane* surface magnetization. This provides a new mechanism for surface magnetization dynamics enabled dynamical magnetoelectric coupling, which further generates a polarization current in the presence of an external magnetic field in the same direction. Such a current measures the finite-size correction to TME, which increases as the film thickness d decreases, in contrast to the TME current, which decreases as d decreases. Remarkably, the current in thin films at magnetic resonance is about several orders of magnitude larger than that of TME, which is absent in trivial insulators and thus could serve as a smoking gun signature for axion insulators. The intimate interplay between surface magnetization dynamics and the magnetoelectric response in the axion insulator phase unveiled here may lead to a new class of electronic and spintronic applications of axion devices.

DOI: [10.1103/PhysRevB.105.214424](https://doi.org/10.1103/PhysRevB.105.214424)

I. INTRODUCTION

The search for new topological phenomena has become an important goal in condensed matter physics [1–3]. The intricate interplay between topology and magnetism could generate a variety of exotic quantum states [4,5]. A prime example is axion insulators (AI), which are magnetic topological insulators (TI) with zero Chern number but a nonzero quantized Chern-Simons magnetoelectric coupling [6–29]. The simplest AI is obtained in three-dimensional (3D) TIs with a surface gap induced by hedgehog magnetization [6,13]. The unique signature of AI is the topological magnetoelectric effect (TME) [6,30–32], where a quantized charge polarization is induced by a parallel magnetic field. Such an electromagnetic response is described by the topological θ term $\mathcal{L}_\theta = (\theta/2\pi)(e^2/h)\mathbf{E} \cdot \mathbf{B}$ [6,33]. Here \mathbf{E} and \mathbf{B} are conventional electromagnetic fields inside the insulator, e is electron charge, h is Planck's constant, and θ is the dimensionless pseudoscalar axion field [34]. In AI, $\theta = \pi$ describes a half-quantized surface anomalous Hall effect, which is the physical origin of TME, image magnetic monopole [35], and topological magneto-optical effect [36–38]. Up to now, no direct experimental confirmation of TME has been achieved due to its small signal, although successful realization of AI candidates is strongly suggested in the ferromagnet-TI-ferromagnet (FM-TI-FM) heterostructure [15–17] and MnBi_2Te_4 [27,28] by the absence of the Hall effect together with a large longitudinal resistance [13]. However, zero Hall resistance can also exist in trivial insulators and is not conclusive. Therefore,

seeking a testable transport signature for AI is still an open question.

An intriguing physical phenomena driven by the topological term is the electromagnetic effect via the dynamics of θ (i.e., $\partial_t\theta$). So far, axion polariton [14] and axion instability [39] were proposed under a nonzero $\partial_t\theta$, for example, in the dynamical axion insulator, where θ dynamics is caused by the intrinsic magnetic fluctuations in 3D bulk materials with breaking time-reversal \mathcal{T} and inversion \mathcal{P} symmetries [14]. Quite differently in 3D AI such as MnBi_2Te_4 , $\theta = \pi$ is protected by \mathcal{P} and is *static*, and to the linear order, the intrinsic magnetic fluctuations have no contributions to the dynamics of θ [21,40]. Therefore, we need to seek other mechanisms to induce θ dynamics in AI.

In this paper, we demonstrate that the finite-size correction to exact quantized θ in AI thin films depends on the out-of-plane surface magnetization, which is enhanced when surface magnetization is weakened. Thus $\partial_t\theta$ is induced by out-of-plane surface magnetization dynamics, which further generates a current in the presence of a magnetic field as shown in Fig. 1(a). Such a current measures finite-size correction to TME, and is much larger than the TME current at magnetic resonance. Interestingly, the current increases as the film thickness d decreases, which perfectly fits with the AI phase of limited d in experiments [15–17,27,28].

The idea can be understood from response current density induced by the θ term

$$\mathbf{j} = \frac{e^2}{2\pi h} [\nabla\theta \times \mathbf{E} + \partial_t\theta\mathbf{B}], \quad (1)$$

where $\partial_t\theta$ induces a polarization current in insulators and is regarded as a kind of chiral magnetic effect [41–46]. Previous studies on TME showed $[1 - \theta(d)/\pi] \propto 1/d$ [13,47]. We

*wjingphys@fudan.edu.cn

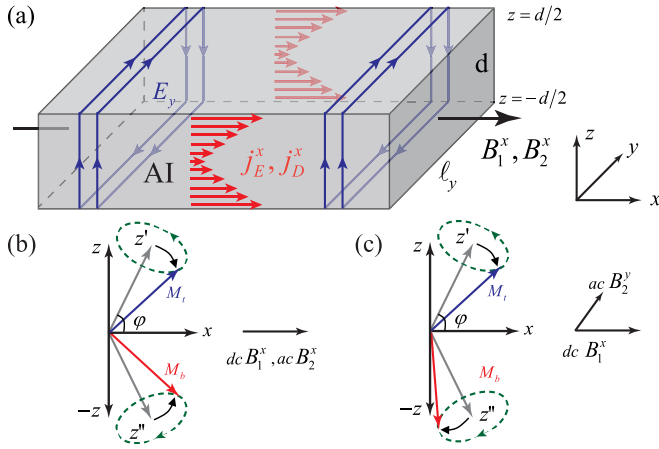


FIG. 1. (a) Illustration of j_E^x and j_D^x , induced by ac field $B_2^x \cos(\omega t)$ and dc field B_1^x . j_E^x and j_D^x are induced by $\nabla\theta$ and $\partial_t\theta$, respectively. The top and bottom surface layers have opposite magnetization (not explicitly shown) in AI. (b) Néel-type and (c) FM-type oscillations from magnetic resonance in different configurations. The antiparallel magnetization along $\pm z$ axis on top and bottom layers now tilt along z' and z'' .

envisaged that hybridization and θ depend on the surface-state exchange gap from out-of-plane surface magnetization M_z , which is now confirmed by numerical calculations here. Therefore $\partial_t\theta$ can be driven by $M_z(t)$ from magnetic resonance.

II. θ VERSUS M_z

First, we examine theoretically the dependence of θ on surface M_z in AI films. For the FM-TI-FM heterostructure and MnBi_2Te_4 with a finite thickness along the z axis, the linear magnetoelectric (ME) response is diagonal but anisotropic, namely $\alpha_{zz} \neq \alpha_{\parallel}$ [47]. Here α_{zz} and α_{\parallel} are the perpendicular and parallel components of the magnetoelectric susceptibility tensor α_{ii} , which relates polarization and the magnetic field according to $P_i = -\alpha_{ii}B_i$, $i = x, y, z$. To avoid confusion, we are interested only in the orbital magnetoelectric polarizability [6–8] with topological character in α_{ii} . The TME response is calculated with the Kubo formula [13,47,48] and is defined as the pseudoscalar axion part

$$(\theta/2\pi)(e^2/h) = (2\alpha_{\parallel} + \alpha_{zz})/3. \quad (2)$$

The generic Hamiltonian of AI films is written as $\mathcal{H}_{2D}(\mathbf{k}) = \int_{-d/2}^{d/2} dz \mathcal{H}_{3D}(\mathbf{k}, z)$. $\mathbf{k} \equiv (k_x, k_y)$. The physical effects discussed here are generic for any AI films. For concreteness, we adopt the effective Hamiltonian in Ref. [21] to describe the low-energy bands of MnBi_2Te_4 (which is the same for FM-TI-FM heterostructure). It has Van der Waals coupled septuple layers (SL) and develops A -type antiferromagnetic (AFM) order with an out-of-plane easy axis, which is ferromagnetic (FM) within each SL but AFM between adjacent SL along the z axis. The $\theta = \pi$ in bulk MnBi_2Te_4 is protected by \mathcal{P} . In the even SL film, \mathcal{T}, \mathcal{P} are broken and thus $\theta \neq \pi$. $\mathcal{H}_{3D}(\mathbf{k}, z) = \varepsilon_1 \otimes 1 + d^1 \tau_1 \otimes \sigma_2 - d^2 \tau_1 \otimes \sigma_1 + d^3 \tau_3 \otimes 1 - \Delta(z) 1 \otimes \sigma_3 - iA_1 \partial_z \tau_1 \otimes \sigma_3$. Here τ_j and σ_j ($j = 1, 2, 3$)

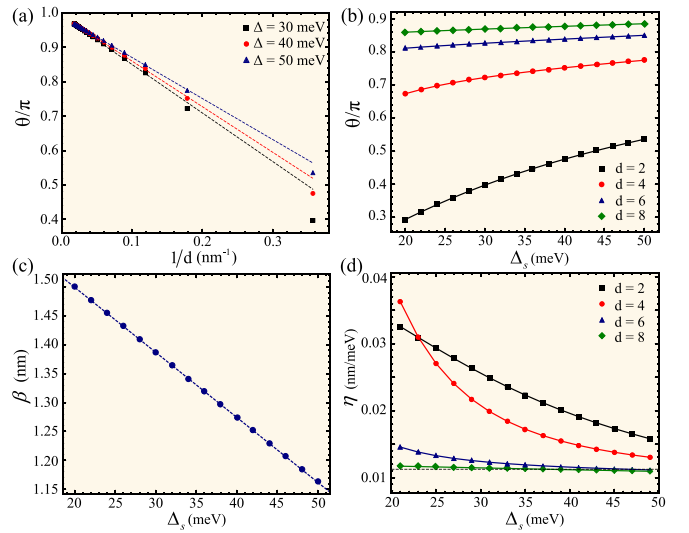


FIG. 2. (a) Finite-size effect of TME. $\theta(d)/\pi$ versus $1/d$ with different typical values of Δ_s . (b) θ/π versus Δ_s for different thickness 2, 4, 6, and 8 SL. (c) β ($d \geq 6$ SL) versus Δ_s . (d) η versus Δ_s . The value of dashed line is $-\partial\beta/\partial\Delta_s$. Each SL is about 1.4-nm thick.

are Pauli matrices, $\varepsilon(\mathbf{k}, z) = -D_1 \partial_z^2 + D_2(k_x^2 + k_y^2)$, $d^{1,2,3}(\mathbf{k}, z) = [A_2 k_x, A_2 k_y, B_0 - B_1 \partial_z^2 + B_2(k_x^2 + k_y^2)]$, and $\Delta(z)$ is the z -dependent exchange field along the z axis. The exchange field in the xy plane will not affect the top and bottom surface gaps and thus is neglected. We assume $\Delta(z)$ takes finite values $\pm\Delta_s$ only in the top and bottom layers due to antiparallel magnetization and zero elsewhere. Explicitly, $\Delta_s = g_M M_z$, where the exchange coupling parameter g_M is assumed to be positive and the same on both surfaces. All other parameters are taken from Ref. [21] for MnBi_2Te_4 (similar results in Bi_2Te_3 family materials).

Figure 2(a) shows the numerical calculations of $\theta(d)$ as a function of $1/d$ for different values of Δ_s . Interestingly, we find the value of $1 - \theta(d)/\pi$ scales linearly with $1/d$ as the thickness $d \geq 6$ SL, while the coefficient depends on Δ_s , which suggests

$$1 - \theta(d)/\pi = \beta(\Delta_s, d)/d. \quad (3)$$

As shown explicitly in Fig. 2(a), when $d \geq 6$ SL, β is independent of d and is a nonuniversal lengthscale of about 1.5 nm, which decreases linearly as Δ_s increases shown in Fig. 2(c). Only for $d \leq 4$ SL does β depend on d and deviates from the value of β ($d \geq 6$ SL), which characterizes the deviation of $1 - \theta(d)/\pi$ from perfect $1/d$ scaling at small d [48]. Figure 2(b) shows $\theta(d)$ is a monotonically increasing function of Δ_s for thin films of 2, 4, 6, and 8 SL. This is consistent with the fact that TME response is from the massive Dirac surface states, and hybridization between the top and bottom surface states partially cancels each others' contributions to TME, which further deviate θ from quantization. Thus the reduced hybridization from more localized surface states with increased Δ_s will lead θ closer to quantization. Now we established the fact that $\theta(d)$ depends on Δ_s . Therefore, the dynamics of Δ_s from magnetic resonance will definitely

induce the dynamics of $\theta(d)$ in AI. Explicitly, we get

$$\partial_t \theta(d) = [\partial \theta(d) / \partial \Delta_s] \partial_t \Delta_s = \pi \eta g_M \partial_t M_z / d, \quad (4)$$

where $\eta \equiv (d/\pi)(\partial \theta / \partial \Delta_s)$. Figure 2(d) shows the numerical calculations of η as a function of Δ_s for different d . We can see that $\eta \rightarrow -\partial \beta / \partial \Delta_s$ quickly converges for thick films when $d \geq 6$ SL, which is consistent with that β is independent of $d \geq 6$ SL in Eq. (3). Now we see $\partial_t \theta$ indeed can be driven by the magnetization M_z dynamics on surfaces, but it vanishes when $d \rightarrow \infty$. It is worth mentioning that Eq. (4) implicitly requires the top and bottom surfaces having opposite M_z , namely the Néel-type oscillation in Fig. 1(b). Furthermore, we point out the essential difference of the magnetization dynamics enabled dynamical θ between AI films and dynamical axion AFM materials. The dynamical magnetoelectric coupling θ in AI films here is due to the finite-size correction of TME and vanishes in the bulk $d \rightarrow \infty$ limit, as demonstrated in Eq. (4), specifically the magnetization dynamics is from surfaces only; while the dynamical θ in the dynamical axion insulator is caused by the intrinsic magnetic fluctuations in the bulk and is finite as $d \rightarrow \infty$ [14], which cannot be excited solely by the surface magnetization dynamics.

III. j_E VERSUS j_D

Now we study the response current from the spatial and temporal gradients of θ in Eq. (1). They are the two sides of the same coin demonstrating TME. Considering the process of applying a uniform dc magnetic field $B_1^x \hat{x}$ and ac field $B_2^x \cos(\omega t) \hat{x}$ of frequency $\omega/2\pi$ in Fig. 1(a). The oscillating B_2^x can induce a nonuniform electric field along y due to Faraday's law: $\mathbf{E}(t, z) = -\omega B_2^x \sin(\omega t) z \hat{y}$ with $z = 0$ set at the middle of the AI layer. From the first term in Eq. (1), this further induces a Hall current density $j_E^x = (\partial_z \theta / 2\pi) (e^2/h) \hat{z} \times \mathbf{E}$. Thus the integration over z gives TME current density in two dimensions,

$$\mathcal{J}_E = \mathcal{J}_E^x \hat{x} = (\theta/2\pi) (e^2/h) \omega d B_2^x \sin(\omega t) \hat{x}, \quad (5)$$

whose amplitude is proportional to θ and limited by d . Here d is maximally 10 nm in experiments to ensure the full insulating state [15–17,27,28]. With typical parameters $B_2^x = 5$ G, $\omega/2\pi = 7$ GHz, $d = 5.6$ nm, $\theta/\pi \approx 0.7$, and $\ell_y = 500 \mu\text{m}$ (the length of film along y), the amplitude of the TME current is $I_E^x = |\max(\mathcal{J}_E^x)| \ell_y = 0.83$ nA, which is quite small to be measured.

Meanwhile, the surface magnetic moments are tilted away from the $\pm z$ axis by B_1^x and B_2^x induces an oscillating M_z with the same frequency. One can decompose M_z into the static and dynamical parts as $M_z = M_0^z + \delta M_z(t)$. In Fig. 1(a) in the configuration dubbed as the Néel-type oscillation, the top and bottom surfaces have opposite $\delta M_z(t)$. Thus the two-dimensional (2D) current density \mathcal{J}_D induced by $\partial_t \theta$ is

$$\mathcal{J}_D = \mathcal{J}_D^x \hat{x} = \frac{e^2}{2h} \eta g_M \partial_t \delta M_z [B_1^x + B_2^x \cos(\omega t)] \hat{x}, \quad (6)$$

whose amplitude is proportional to η and thus increases as d decreases, in sharp contrast to \mathcal{J}_E , which decreases as d decreases. There are ω and 2ω components in \mathcal{J}_D^x , which are proportional to B_1^x and B_2^x , respectively. In particular, for finite films, the 2ω component $\mathcal{J}_D^x(2\omega)/\mathcal{J}_E^x = \delta\theta/\theta < 0.1$,

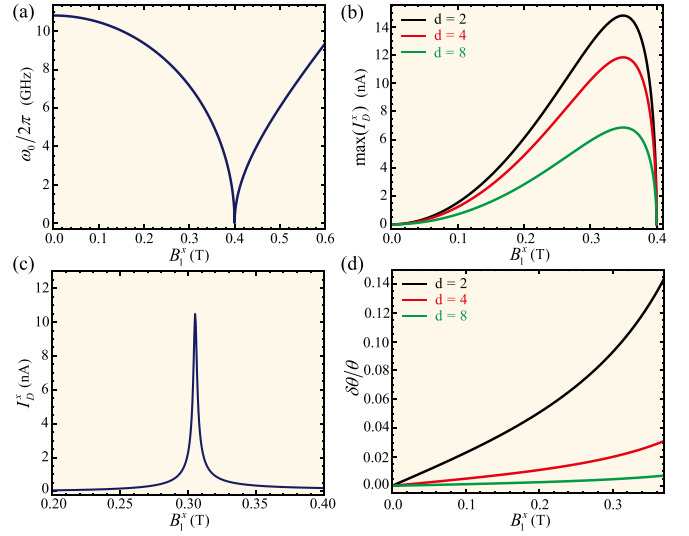


FIG. 3. FMR. (a) The FMR frequency $\omega_0/2\pi$ versus B_1^x . (b) The resonant amplitude of $I_D^x = |\max(\mathcal{J}_D^x)| \ell_y$ at FMR versus B_1^x for 2, 4, and 8 SL. (c) The response of I_D^x amplitude versus B_1^x for 4 SL, with the frequency fixed at $\omega/2\pi = 7$ GHz. (d) $\delta\theta/\theta$ versus B_1^x . Here $K = 2 \times 10^4$ J/m³, $M_s = 10^5$ A/m, and $\alpha = 5 \times 10^{-3}$.

with $\delta\theta \equiv (\partial \theta / \partial \Delta_s) g_M \delta M_z$ the oscillating part in θ due to δM_z . $\delta\theta/\theta \approx 0.01 \sim 0.1$ as calculated in Fig. 3(d). Therefore, $\mathcal{J}_D^x(2\omega)$ can be neglected. In the following we focus on only $\mathcal{J}_D^x(\omega)$.

IV. FMR-INDUCED δM_z

First we consider the M_z dynamics induced by FM resonance (FMR) in the FM-TI-FM heterostructure. The tilted magnetization is along z' (z''), where the angle between z' (z'') and the x axis is φ as shown in Fig. 1(b). $\cos \varphi = B_1^x M_s / 2K$, $M_s = |\mathbf{M}|$ is the saturation magnetization, K is the effective uniaxial anisotropy. Here we consider $\varphi \neq 0$ to ensure it is always in the AI phase. The two FM layers are decoupled, and the magnetization dynamics governed by the Landau-Lifshitz-Gilbert (LLG) equations [49,50] for two FM layers under the same $B_2^x(t)$ have the same form. For simplicity, we assume the damping constant and M_s are the same in two FM layers. The equation is solved by linearization [48,49], the steady solution of δM_z at FMR is given by

$$\delta M_z = \frac{\gamma \omega_1 B_2^x M_s \sin 2\varphi}{2\alpha \omega_0 (2\omega_1 - \gamma B_1^x \cos \varphi)} \sin(\omega_0 t), \quad (7)$$

where $\gamma = \gamma_0 / (1 + \alpha^2)$, $\gamma_0 = 2e / (2m_e)$ is the gyromagnetic ratio of an electron, α is the dimensionless Gilbert damping constant, $\omega_0 = \sqrt{\omega_1 (\omega_1 - \gamma B_1^x \cos \varphi)}$ is the resonance frequency, $\omega_1 = \gamma (B_1^x \cos \varphi + 2K \sin^2 \varphi / M_s)$. Obviously, $\delta M_z \neq 0$ when $\varphi \neq \pi/2$. The adiabatic approximation always holds, for the energy scale of the typical FMR frequency range $\omega_0/2\pi = 1 \sim 10$ GHz is much smaller than the surface magnetic gap. Then the 2D current density \mathcal{J}_D^x at FMR is

$$\mathcal{J}_D^x = \frac{e^2}{2h} \frac{\gamma B_1^x B_2^x \eta g_M M_s \omega_1 \sin 2\varphi}{2\alpha (2\omega_1 - \gamma B_1^x \cos \varphi)} \cos(\omega_0 t). \quad (8)$$

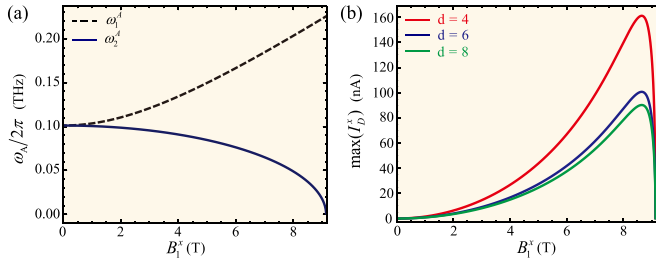


FIG. 4. AFMR. (a) Two branches of AFMR frequency $\omega_A/2\pi$ versus B_1^x . (b) The amplitude of I_D^x at AFMR in the ω_2^A branch versus B_1^x for 4, 6, and 8 SL and that in the ω_1^A branch almost vanishes (not shown).

With a fixed ω , one can scan B_1^x to achieve FMR. The resonant frequency of the FM layer ω_0 versus B_1^x is calculated in Fig. 3(a), where $\omega_0 = 0$ represents the magnetization is just tuned to be in-plane, namely, $\varphi = 0$. With similar typical parameters $B_2^x = 5$ G, $d = 5.6$ nm, $\ell_y = 500$ μm , and $\alpha = 5 \times 10^{-3}$ in FM [51], then the estimated amplitude of I_D^x versus B_1^x is shown in Fig. 3(b), where the maximum value is about 12 nA, in the range accessible by transport experiments.

We compare the ratio between the amplitudes of \mathcal{J}_D^x and \mathcal{J}_E^x as $\mathcal{R} \equiv |\max(\mathcal{J}_D^x)/\max(\mathcal{J}_E^x)| = (\delta\theta/\theta)(B_1^x/B_2^x)$. With $\delta\theta/\theta \approx 0.01 \sim 0.1$, and $B_1^x = 0.1 \sim 0.4$ T, the ratio is approximately $\mathcal{R} \approx 10^1 \sim 10^2$. Thus \mathcal{J}_D at FMR is the dominant contribution. Importantly, it is larger in thin film than that in the thick one, which fits well with the experimental condition of limited d . Moreover, TME vanishes for the thin films of trivial insulating states (bulk $\theta = 0$). Therefore, I_D^x can be used to distinguish AI from a trivial insulator experimentally.

V. AFMR-INDUCED δM_z

Then we study $\partial_t M_z$ induced by AFM resonance (AFMR) in AI such as MnBi_2Te_4 . This is the simplest bipartite collinear AFM, where the magnetic dynamics of surface M_z is governed by Landau—Lifshitz—Gilbert (LLG) equations by including the exchanging coupling term between neighboring SL due to the intrinsic magnetism. The tilted magnetization is along z' (z'') with the angle φ between z' (z'') and x , but now $\cos\varphi = B_1^x/(4B_E + 2B_A)$, where $B_E \equiv J_A M_s$ and $B_A \equiv K_1/M_s$ are the exchange field and anisotropy field, respectively. The equations are solved by linearization and numerically [48]. Taking the exchange coupling $J_A = 0.55$ meV, the effective anisotropy field $K_1 = 0.22$ meV [52,53], $\alpha = 5 \times 10^{-3}$, $M_s = 2 \times 10^5$ A/m, $B_2^x = 5$ G, the AFMR frequency ω_A versus B_1^x is shown in Fig. 4(a). The two branches ω_1^A and ω_2^A represent the resonance from AFM and FM components, respectively. The estimated I_D^x amplitude is calculated in Fig. 4(b), where the maximum value is about 100 nA in the ω_2^A branch, and is negligible in the ω_1^A branch. Then the ratio between \mathcal{J}_D^x and \mathcal{J}_E^x is about $\mathcal{R} \approx 1 \sim 20$.

VI. DIFFERENT CONFIGURATION

Then we discuss the Fig. 1(c) configuration where $B_2^y \cos(\omega t)\hat{y}$ is applied along the y axis, but keeping $B_1^x\hat{x}$ along the x axis. The top and bottom surfaces now have the same oscillating $\delta M_z(t)$ induced by B_2^y for both FMR and AFMR

[48], and is dubbed as FM-type oscillation. We find θ almost unchanged by varying δM_z , specifically, $\delta\theta/\theta$ is vanishingly smaller compared to that from the Néel-type oscillation [48]. Therefore, \mathcal{J}_D^x almost vanishes compared to \mathcal{J}_E^y in the new configuration, which provides another testable signature for our theory.

VII. DISCUSSION

Our theory is fundamentally different from the pseudo-electric field induced current \mathcal{J}_F discussed in Ref. [54]. In Ref. [54], \mathcal{J}_F is from the first term in Eq. (1), where the pseudo-electric field is induced by in-plane magnetization dynamics. \mathcal{J}_F is always along the ac-field (B_2) direction and is maximized when magnetization is oscillating around the z axis; while in our case, \mathcal{J}_D is from the second term in Eq. (1), where $\partial_t\theta$ is driven by the out-of-plane surface magnetization dynamics. \mathcal{J}_D is along the dc-field (B_1) direction and is maximized when magnetization is tilted far away from the z axis and close to the x axis. Also, \mathcal{J}_F is proportional to θ , which decreases as d decreases, similarly to the TME current; while the thickness dependence of \mathcal{J}_D in our case is just the opposite, namely, \mathcal{J}_D increases as d decreases. The different dependence of \mathcal{J}_D and \mathcal{J}_F on tilting angle φ (thus dc-field B_1^x) and thickness d will help to separate them experimentally. In Fig. 1(c) configuration, \mathcal{J}_D^x vanishes even as B_1^x is finite, while \mathcal{J}_F^y is along the y axis and is finite. While in the Fig. 1(b) configuration, both \mathcal{J}_D^x and \mathcal{J}_F^x are finite and along the x axis. For an estimation, with the same parameters in Fig. 3(b) and in typical $d = 4$ SL, the ratio of the resonant current amplitude $I_D^x/I_F^x = 12\text{nA}/2\text{nA}$ when $B_1^x = 0.35$ T, while $I_D^x/I_F^x = 0\text{nA}/5\text{nA}$ when $B_1^x = 0$ T. The detailed resonant current I_D^x and I_F^x at FMR versus B_1^x is shown in the Supplemental Material [48]. The increasing of the total current along the x axis at finite B_1^x is purely from I_D^x . We find I_F^x in the Fig. 1(b) configuration is equal to I_F^y in the Fig. 1(c) configuration; then one can further separate I_D^x and I_F^x by combining the measurements in both Figs. 1(b) and 1(c), namely $I_D^x = I_{\text{total}}^x - I_F^y$ [48].

Interestingly, there is another configuration which can separate \mathcal{J}_D and \mathcal{J}_F qualitatively. It is a parallel magnetization configuration in the FM-TI-FM heterostructure realizing the AI state, when the top and bottom layers have opposite signs of exchange coupling parameters [55]. This can be achieved experimentally by using Mn-doped [28,56] and Cr-doped or V-doped [17] Bi_2Te_3 as the top and bottom magnetic layers, respectively. In this parallel configuration, FMR excited by the ac field on both layers is exactly the same, \mathcal{J}_F is along the ac-field direction and almost vanishes [48], while \mathcal{J}_D is finite and along the dc field and is independent of the ac-field direction. Thus an orthogonal ac-field and dc-field measurement scheme will separate \mathcal{J}_D and \mathcal{J}_F experimentally.

Finally, we briefly discuss the experimental feasibility. \mathcal{J}_D can be measured by capacitive sensing. For a measurable current of about 10 nA, the needed power of antenna for FM resonance may be stringent, while it is feasible for AFM resonance. The low-ordering temperature of AI in the FM-TI-FM heterostructure or MnBi_2Te_4 limits the compatibility between cryostat and radiation power. However, the theoretical proposal here is generic for any AI state. Thus, improved

material quality as well as new topological AI materials would release such limitations. Moreover, a different measurement configuration and giant current in the AFM resonance would differentiate \mathcal{J}_D from the parasitic effect.

VIII. SUMMARY

Instead of measuring the long-sought after TME current, we propose to measure a dynamical magnetoelectric current from the finite-size correction to TME, which is about one-to-two orders of magnitude larger than the TME current at FMR in AI films. Such a current is absent in trivial insulators and could serve as a smoking-gun signature for AI. Recently, FMR was observed in the FM-TI heterostructure [51], making the magnetoelectric current in AI films predicted here feasible. Our theory unveils a generic and intimate interplay between

surface magnetization dynamics and the magnetoelectric response in AI, which is expected to have a great impact for electronic and spintronic applications of axion devices.

ACKNOWLEDGMENTS

We acknowledge B. Lian, Y. Wu, and Y. Wang for valuable discussions. This work is supported by the National Key Research Program of China under Grants No. 2019YFA0308404 and No. 2016YFA0300703; the Natural Science Foundation of China through Grants No. 11774065, No. 12174066, and No. 11722430; the Science and Technology Commission of Shanghai Municipality under Grant No. 20JC1415900; the Shanghai Municipal Science and Technology Major Project under Grant No. 2019SHZDZX01; and the Natural Science Foundation of Shanghai under Grant No. 19ZR1471400.

-
- [1] D. J. Thouless, *Topological Quantum Numbers in Nonrealistic Physics* (World Scientific, Singapore, 1998).
- [2] M. Z. Hasan and C. L. Kane, *Colloquium: Topological insulators*, *Rev. Mod. Phys.* **82**, 3045 (2010).
- [3] X.-L. Qi and S.-C. Zhang, Topological insulators and superconductors, *Rev. Mod. Phys.* **83**, 1057 (2011).
- [4] Y. Tokura, K. Yasuda, and A. Tsukazaki, Magnetic topological insulators, *Nat. Rev. Phys.* **1**, 126 (2019).
- [5] J. Wang and S.-C. Zhang, Topological states of condensed matter, *Nat. Mater.* **16**, 1062 (2017).
- [6] X.-L. Qi, T. L. Hughes, and S.-C. Zhang, Topological field theory of time-reversal invariant insulators, *Phys. Rev. B* **78**, 195424 (2008).
- [7] A. M. Essin, J. E. Moore, and D. Vanderbilt, Magnetoelectric Polarizability and Axion Electrodynamics in Crystalline Insulators, *Phys. Rev. Lett.* **102**, 146805 (2009).
- [8] S. Coh, D. Vanderbilt, A. Malashevich, and I. Souza, Chern-Simons orbital magnetoelectric coupling in generic insulators, *Phys. Rev. B* **83**, 085108 (2011).
- [9] K. Nomura and N. Nagaosa, Surface-Quantized Anomalous Hall Current and the Magnetoelectric Effect in Magnetically Disordered Topological Insulators, *Phys. Rev. Lett.* **106**, 166802 (2011).
- [10] A. M. Turner, Y. Zhang, R. S. K. Mong, and A. Vishwanath, Quantized response and topology of magnetic insulators with inversion symmetry, *Phys. Rev. B* **85**, 165120 (2012).
- [11] X. Wan, A. Vishwanath, and S. Y. Savrasov, Computational Design of Axion Insulators Based on 5d Spinel Compounds, *Phys. Rev. Lett.* **108**, 146601 (2012).
- [12] T. Morimoto, A. Furusaki, and N. Nagaosa, Topological magnetoelectric effects in thin films of topological insulators, *Phys. Rev. B* **92**, 085113 (2015).
- [13] J. Wang, B. Lian, X.-L. Qi, and S.-C. Zhang, Quantized topological magnetoelectric effect of the zero-plateau quantum anomalous Hall state, *Phys. Rev. B* **92**, 081107(R) (2015).
- [14] R. Li, J. Wang, X. L. Qi, and S. C. Zhang, Dynamical axion field in topological magnetic insulators, *Nat. Phys.* **6**, 284 (2010).
- [15] M. Mogi, M. Kawamura, R. Yoshimi, A. Tsukazaki, Y. Kozuka, N. Shirakawa, K. S. Takahashi, M. Kawasaki, and Y. Tokura, A magnetic heterostructure of topological insulators as a candidate for an axion insulator, *Nat. Mater.* **16**, 516 (2017).
- [16] M. Mogi, M. Kawamura, A. Tsukazaki, R. Yoshimi, K. S. Takahashi, M. Kawasaki, and Y. Tokura, Tailoring tricolor structure of magnetic topological insulator for robust axion insulator, *Sci. Adv.* **3**, eaao1669 (2017).
- [17] D. Xiao, J. Jiang, J.-H. Shin, W. Wang, F. Wang, Y.-F. Zhao, C. Liu, W. Wu, M. H. W. Chan, N. Samarth, and C.-Z. Chang, Realization of the Axion Insulator State in Quantum Anomalous Hall Sandwich Heterostructures, *Phys. Rev. Lett.* **120**, 056801 (2018).
- [18] S. Grauer, K. M. Fijalkowski, S. Schreyeck, M. Winnerlein, K. Brunner, R. Thomale, C. Gould, and L. W. Molenkamp, Scaling of the Quantum Anomalous Hall Effect as an Indicator of Axion Electrodynamics, *Phys. Rev. Lett.* **118**, 246801 (2017).
- [19] N. Varnava and D. Vanderbilt, Surfaces of axion insulators, *Phys. Rev. B* **98**, 245117 (2018).
- [20] M. Allen, Y. Cui, E. Yue Ma, M. Mogi, M. Kawamura, I. C. Fulga, D. Goldhaber-Gordon, Y. Tokura, and Z.-X. Shen, Visualization of an axion insulating state at the transition between 2 chiral quantum anomalous hall states, *Proc. Natl. Acad. Sci. USA* **116**, 14511 (2019).
- [21] D. Zhang, M. Shi, T. Zhu, D. Xing, H. Zhang, and J. Wang, Topological Axion States in the Magnetic Insulator MnBi_2Te_4 with the Quantized Magnetoelectric Effect, *Phys. Rev. Lett.* **122**, 206401 (2019).
- [22] Y. Gong, J. Guo, J. Li, K. Zhu, M. Liao, X. Liu, Q. Zhang, L. Gu, L. Tang, X. Feng, D. Zhang, W. Li, C. Song, L. Wang, P. Yu, X. Chen, Y. Wang, H. Yao, W. Duan, Y. Xu, S.-C. Zhang, X. Ma, Q.-K. Xue, and K. He, Experimental realization of an intrinsic magnetic topological insulator, *Chin. Phys. Lett.* **36**, 076801 (2019).
- [23] X. Gui, I. Pletikoscic, H. Cao, H.-J. Tien, X. Xu, R. Zhong, G. Wang, T.-R. Chang, S. Jia, T. Valla, W. Xie, and R. J. Cava, A new magnetic topological quantum material candidate by design, *ACS Cent. Sci.* **5**, 900 (2019).
- [24] Y. Xu, Z. Song, Z. Wang, H. Weng, and X. Dai, Higher-Order Topology of the Axion Insulator EuIn_2As_2 , *Phys. Rev. Lett.* **122**, 256402 (2019).
- [25] S. Chowdhury, K. F. Garrity, and F. Tavazza, Prediction of weyl semimetal and antiferromagnetic topological insulator phases in Bi_2MnSe_4 , *npj Comput. Mater.* **5**, 33 (2019).
- [26] B. J. Wieder and B. A. Bernevig, The axion insulator as a pump of fragile topology, [arXiv:1810.02373](https://arxiv.org/abs/1810.02373).

- [27] C. Liu, Y. Wang, H. Li, Y. Wu, Y. Li, J. Li, K. He, Y. Xu, J. Zhang, and Y. Wang, Robust axion insulator and chern insulator phases in a two-dimensional antiferromagnetic topological insulator, *Nat. Mater.* **19**, 522 (2020).
- [28] Y. Deng, Y. Yu, M. Z. Shi, Z. Guo, Z. Xu, J. Wang, X. H. Chen, and Y. Zhang, Quantum anomalous hall effect in intrinsic magnetic topological insulator MnBi_2Te_4 , *Science* **367**, 895 (2020).
- [29] N. Varnava, I. Souza, and D. Vanderbilt, Axion coupling in the hybrid wannier representation, *Phys. Rev. B* **101**, 155130 (2020).
- [30] A. Karch, Electric-Magnetic Duality and Topological Insulators, *Phys. Rev. Lett.* **103**, 171601 (2009).
- [31] M. Mulligan and F. J. Burnell, Topological insulators avoid the parity anomaly, *Phys. Rev. B* **88**, 085104 (2013).
- [32] H.-G. Zirnstein and B. Rosenow, Time-reversal-symmetric topological magnetoelectric effect in three-dimensional topological insulators, *Phys. Rev. B* **96**, 201112(R) (2017).
- [33] F. Wilczek, Two Applications of Axion Electrodynamics, *Phys. Rev. Lett.* **58**, 1799 (1987).
- [34] R. D. Peccei and H. R. Quinn, CP Conservation in the Presence of Pseudoparticles, *Phys. Rev. Lett.* **38**, 1440 (1977).
- [35] X.-L. Qi, R. Li, J. Zang, and S.-C. Zhang, Seeing the magnetic monopole through the mirror of topological surface states, *Science* **323**, 1184 (2009).
- [36] K. N. Okada, Y. Takahashi, M. Mogi, R. Yoshimi, A. Tsukazaki, K. S. Takahashi, N. Ogawa, M. Kawasaki, and Y. Tokura, Terahertz spectroscopy on faraday and kerr rotations in a quantum anomalous hall state, *Nat. Commun.* **7**, 12245 (2016).
- [37] L. Wu, M. Salehi, N. Koirala, J. Moon, S. Oh, and N. P. Armitage, Quantized faraday and kerr rotation and axion electrodynamics of a 3d topological insulator, *Science* **354**, 1124 (2016).
- [38] V. Dziom, A. Shuvaev, A. Pimenov, G. V. Astakhov, C. Ames, K. Bendias, J. Böttcher, G. Tkachov, E. M. Hankiewicz, C. Brüne, H. Buhmann, and L. W. Molenkamp, Observation of the universal magnetoelectric effect in a 3d topological insulator, *Nat. Commun.* **8**, 15197 (2017).
- [39] H. Ooguri and M. Oshikawa, Instability in Magnetic Materials with a Dynamical Axion Field, *Phys. Rev. Lett.* **108**, 161803 (2012).
- [40] J. Zhang, D. Wang, M. Shi, T. Zhu, H. Zhang, and J. Wang, Large dynamic axion field in topological antiferromagnetic insulator $\text{Mn}_2\text{Bi}_2\text{Te}_5$, *Chin. Phys. Lett.* **37**, 077304 (2020).
- [41] K. Fukushima, D. E. Kharzeev, and H. J. Warringa, Chiral magnetic effect, *Phys. Rev. D* **78**, 074033 (2008).
- [42] M. M. Vazifeh and M. Franz, Electromagnetic Response of Weyl Semimetals, *Phys. Rev. Lett.* **111**, 027201 (2013).
- [43] A. A. Zyuzin and A. A. Burkov, Topological response in weyl semimetals and the chiral anomaly, *Phys. Rev. B* **86**, 115133 (2012).
- [44] A. Sekine and K. Nomura, Chiral Magnetic Effect and Anomalous Hall Effect in Antiferromagnetic Insulators with Spin-Orbit Coupling, *Phys. Rev. Lett.* **116**, 096401 (2016).
- [45] K. Taguchi, T. Imaeda, T. Hajiri, T. Shiraishi, Y. Tanaka, N. Kitajima, and T. Naka, Electromagnetic effects induced by a time-dependent axion field, *Phys. Rev. B* **97**, 214409 (2018).
- [46] N. P. Armitage, E. J. Mele, and A. Vishwanath, Weyl and dirac semimetals in three-dimensional solids, *Rev. Mod. Phys.* **90**, 015001 (2018).
- [47] Z. Liu and J. Wang, Anisotropic topological magnetoelectric effect in axion insulators, *Phys. Rev. B* **101**, 205130 (2020).
- [48] See Supplemental Material at <http://link.aps.org/supplemental/10.1103/PhysRevB.105.214424> for technical details.
- [49] C. Kittel, On the theory of ferromagnetic resonance absorption, *Phys. Rev.* **73**, 155 (1948).
- [50] D. C. Mattis, *The Theory of Magnetism I: Statics and Dynamics* (Springer, Berlin, 1988).
- [51] T. Liu, J. Kally, T. Pillsbury, C. Liu, H. Chang, J. Ding, Y. Cheng, M. Hilsse, R. Engel-Herbert, A. Richardella, N. Samarth, and M. Wu, Changes of Magnetism in a Magnetic Insulator due to Proximity to a Topological Insulator, *Phys. Rev. Lett.* **125**, 017204 (2020).
- [52] M. M. Otrokov, I. I. Klimovskikh, H. Bentmann, A. Zeugner, Z. S. Aliev, S. Gass, A. U. B. Wolter, A. ra V. Koroleva, D. Estyunin, A. M. Shikin, M. Blanco-Rey, M. Hoffmann, A. R. Y. Vyazovskaya, S. V. Eremeev, Y. M. Koroteev, I. R. Amiraslanov, M. B. Babanly, N. T. Mamedov, N. A. Abdullayev, V. N. Zverev, A. Alfonso, V. Kataev, B. Büchner, E. F. Schwier, S. Kumar, A. Kimura, L. Petaccia, G. Di Santo, R. C. Vidal, S. Schatz, K. Kißner, M. Ünzelmann, C. H. Min, S. Moser, T. R. F. Peixoto, F. Reinert, A. Ernst, P. M. Echenique, A. Isaeva, and E. V. Chulkov, Prediction and observation of an antiferromagnetic topological insulator, *Nature (London)* **576**, 416 (2019).
- [53] B. Li, J.-Q. Yan, D. M. Pajerowski, E. Gordon, A.-M. Nedić, Y. Sizyuk, L. Ke, P. P. Orth, D. Vaknin, and R. J. McQueeney, Competing Magnetic Interactions in the Antiferromagnetic Topological Insulator MnBi_2Te_4 , *Phys. Rev. Lett.* **124**, 167204 (2020).
- [54] J. Yu, J. Zang, and C.-X. Liu, Magnetic resonance induced pseudoelectric field and giant current response in axion insulators, *Phys. Rev. B* **100**, 075303 (2019).
- [55] J. Wang, B. Lian, and S.-C. Zhang, Dynamical axion field in a magnetic topological insulator superlattice, *Phys. Rev. B* **93**, 045115 (2016).
- [56] J. G. Checkelsky, J. Ye, Y. Onose, Y. Iwasa, and Y. Tokura, Dirac-fermion-mediated ferromagnetism in a topological insulator, *Nat. Phys.* **8**, 729 (2012).